Long-Distance, Multi-Gigabit-Per-Second Terahertz Wireless Communication

1st John F. O'Hara School of Elec. & Comp. Engin. Oklahoma State University Stillwater, OK USA 0000-0001-8193-1867

5th Rajind Mendis Riverside Research Beavercreek, OH USA rmendis@riversidereseasrch.org 2nd Karl L. Strecker School of Elec. & Comp. Engin. Oklahoma State University Stillwater, OK USA karl.l.strecker@okstate.edu

6th Mark D'Agostino Mission Tech. | C5ISR Systsms Huntington-Ingalls Industries Rome, NY USA mark.dagostino@hii-tsd.com 3rd G. Levi Captain School of Elec. & Comp. Engin. Oklahoma State University Stillwater, OK USA george.captain@okstate.edu

7th Joseph Gates Mission Tech. | C5ISR Systsms Huntington-Ingalls Industries Rome, NY USA joseph.gates@hii-tsd.com 4th Forrest Tuschhoff School of Elec. & Comp. Engin. Oklahoma State University Stillwater, OK USA ftuschh@okstate.edu

Abstract—The performance of long-distance, terahertz wireless communication is rapidly improving to the extent that applications such as wireless backhaul are becoming feasible. Nevertheless, the combination of long distance and ultrabroadband operation introduce several unique challenges. We report on a 2.92 km wireless communication link operating at 130 GHz, achieving bit rates over 8 gigabit-per-second using a QPSK modulation scheme. Two different baseband signal generators were tested to qualify both methods. The system employed was built almost entirely from commercially available components. Several practical challenges encountered in this demonstration are discussed.

Keywords-wireless, terahertz, backhaul, 6G, communication

I. Introduction

The demand for higher wireless data rates continues to rapidly grow, along with the problem of spectrum crowding. This has prompted more dedicated research into innovative communication solutions in the terahertz band, defined here between 0.1-10 THz. The benefits of the terahertz band over lower frequencies are numerous, including the availability of large (multi-GHz) spectrum blocks, fiber-like data rates, and smaller antennas – commensurate with smaller wavelengths. The challenges are likewise numerous: higher free-space path loss (FSPL), greater atmospheric absorption, and more stringent beamforming and aiming requirements. In the past, these challenges discouraged researchers from consideration of longdistance terahertz, or even sub-terahertz (0.1-1 THz) communications. However, terahertz technology has now reached a sufficient state of maturation that functional systems are capable, even over long distances (> 1 km) and with multi-GHz (ultrabroadband) bandwidth [1].

One very promising and near-term application of long-distance, ultrabroadband communication is backhaul, where a

Funding support: This work was supported in part by the National Aeronautics and Space Administration, Grant 80NSSC22K0878, and the National Science Foundation, Grant ECCS-2238132.

point-to-point link supports a very large data rate (ref. [1] and references therein) [2][3][4]. Optical fiber is the usual preferred backhaul medium, but there are many situations where it is not practical [5][6][7][8]. For instance, in remote/rural areas, fiber installation may not be economically feasible. In crowded metropolitan areas, fiber installation may be too costly or disruptive. Finally, ad hoc networks for temporary/transient military operations or disaster recovery sites would represent likely cases where fiber installation is impossible. Terahertz backhaul presents an obvious and timely solution in these cases. Using high-gain antennas, terahertz beams can be highly directive, overcoming FSPL, maximizing network security [9] and minimizing multi-path fading. Terahertz waves have been shown to propagate quite freely through fog, dust, and precipitation, unlike optical wireless beams [10][11][12] [13][14]. Finally, the terahertz band is required to access the large bandwidths needed for fiber-like speeds, which are required of a backhaul network.

Despite the growing promise, backhaul demonstrations over large distances are still uncommon and fraught with technical difficulties. High gain antennas with good efficiency are difficult to design and optimize in practice. They also become more sensitive to alignment errors and aiming jitter. The wide bandwidths employed introduce challenging system noise levels and often include spurious signals from non-idealities in the mixing components or amplifiers. The equipment required is still generally bulky, power-hungry, and lacks robustness for outdoor operations. Finally, the transmitted power must be adequate to overcome atmospheric absorption, even in unfavorable weather conditions like hot summer months where water vapor content in the atmosphere is elevated. These challenges must be met and overcome in real-world demonstrations to comprehensively address the bottlenecks in long-distance, ultrabroadband terahertz backhaul.

In this work, we report the demonstration of a terahertz (130±2.73 GHz), multi-gigabit-per-second (up to 8.4 Gbps) link operating over a distance of 2.92 km (1.82 miles). The custom

communication system is almost entirely built from commercial-off-the-shelf (COTS) components including two different software-defined, digital baseband systems. This work illustrates the feasibility of long-distance backhaul links, even in unfavorable weather conditions, and reveals possible improvements to significantly enhance future operations.

II. SYSTEM DESCRIPTION

A. System Architecture

The overall architecture of our system is shown in Figs. 1 and 2. The transmitter module was located on the roof of Boone Pickens Stadium on the campus of Oklahoma State University, at a height of approximately 40 m. This permitted an unobstructed, 2.92 km line of sight (LOS) to the receiver module, which was positioned at the end of a jetty that protrudes into Boomer Lake. The lake surface provided a wide area around the receiver unobstructed by foliage or buildings. The transmitter and receiver modules are described in greater detail in Ref. [15], however the most relevant details are also provided below.



Fig. 1: Line of sight channel of ~3 km link.

B. Transmitter Module

The transmitter module consisted of a 64 gigasample/second (Gsps) arbitrary waveform generator (AWG), a performance signal generator (PSG), and an upconverter. The AWG produced an 8-bit, phase modulated (M-ary phase shift keying (M = 2 and M = 4)), IF signal consisting of a pseudo-random sequence (PRS) of 16,384 samples and occupying up to 5.5 GHz of bandwidth centered at 10 GHz. This signal was continually repeated during transmissions.

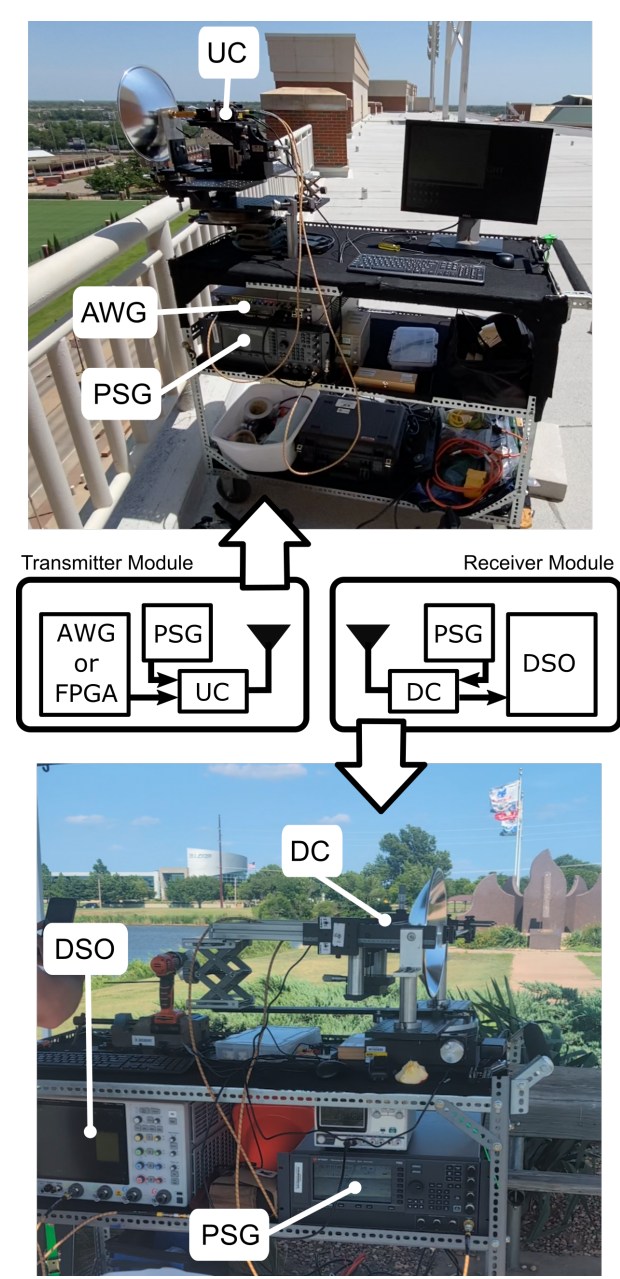


Fig. 2: Transmitter and receiver module hardware. Abbreviations: AWG = arbitrary waveform generator, PSG = performance signal generator, UC = upconverter, DC = downconverter, DSO = digital sampling oscilloscope.

The PSG provided a low phase-noise, stable, local oscillator (LO) at 20 GHz, which fed the upconverter where it was

multiplied ×6 to 120 GHz. This was mixed with the IF signal by the upconverter to produce the terahertz broadcast signal whose upper sideband was centered at 130 GHz.

A high-pass waveguide filter (not shown) was added to the upconverter to eliminate the lower sideband. Two waveguide power amplifiers (also not shown in the block diagram) directly upstream of the antenna together provided ~38 dB of broadband gain.

The AWG signal level fed into the power amplifiers was initially kept low to minimize amplifier compression and nonlinear signal distortions in the transmitter chain, eliminating the need for signal predistortion and minimizing equalization requirements. Using this modest AWG output gain, the radiated power of a continuous-wave alignment tone was measured at 130 GHz using a commercial, calorimeter-style power meter and found to be 24 mW (14 dBm). To achieve greater communication range, the AWG gain was scaled up to the maximum level permissible by the upconverter, resulting in an estimated 84 mW (19 dBm) of radiated output power. Due to amplifier compression, some signal distortion was expected, however it was not observed to a significant extent.

C. Receiver Module

The receiver module consisted of another equivalent PSG, an 80 Gsps digital storage oscilloscope (DSO), and a downconverter. The PSG produced an LO at 20.1666 GHz which was multiplied at the downconverter by ×6 to 121 GHz. This was mixed inside the downconverter with the received terahertz signal to reproduce the IF signal. This IF signal was fed into a "low-noise" amplifier (LNA) – not shown – with 30 dB gain and a 14 dB noise figure before continuing to the DSO. The DSO captured and stored multiple repetitions of the PRS at 40 Gsps for a duration of 1 ms. No attempt was made to synchronize the receiver module to the transmitter module since the off-line software processing that followed data collection was capable of dynamic clock recovery. Using measurements where the transmitter power was set to zero, the noise figure of the receiver chain could be estimated from measurements and was found to be 14 dB (equivalently a system noise temperature of $\sim 7,400 \text{ K}$).

D. Field Programmable Gate Array

To qualify its operation and test any challenges that may result from its use, a field programmable gate array (FPGA) was also employed in place of the AWG to perform baseband signal generation tasks. Since a single RF output channel of the FPGA can support only 3 GHz of bandwidth (6 Gsps sampling rate), the resulting IF signal was likewise limited. The LO frequencies utilized during operations with the FGPA were slightly shifted to minimize aliasing interference produced from image frequencies. Specifically, the transmitter LO was 19 GHz and the receiver LO was 20.5 GHz. Because of these differences, the broadcast carrier frequency for the FPGA-sourced signal was commensurately reduced to 115.6 GHz. It is worth noting that both the AWG and the FPGA were configured to generate signals already at the IF. Consequently, the I and Q channels did not follow separate signal paths, and no IQ imbalance was expected nor observed.

E. Antennas

Both the transmitter and receiver modules utilized custom designed and built Cassegrain antennas to achieve the gain necessary to close the link. Each antenna was combined with a horn antenna attached directly to the waveguide input/output of the downconverter or upconverter amplifiers. The Cassegrain antennas had a nominal design gain of >50 dBi; separate measurements validated the expected directivity of these antennas. However, the actual gain was impaired by efficiency losses due in part to the subreflector blocking the most intense part of the beam. As such, the gain of the antennas was estimated at 48 dBi. Both antennas were mounted on custom gimbal structures to permit precision pointing adjustments in both azimuth and elevation.

III. DATA ANALYSIS

A. Data Processing

Data stored on the DSO were processed offline in software. IF signals were first digitally mixed coarsely to baseband and re-sampled to reduce the computational burden in subsequent processing steps and to provide a more direct comparison to the transmitted signal. Because our receiver and transmitter were not synchronized, the receiver IF exhibited drift which had to be eliminated before demodulation. This was done in MATLAB by means of the built-in carrier synchronization system object, which is an implementation of a digital closed-loop frequency compensator. Technical details are available in the MATLAB documentation and in [16].

After carrier synchronization, timing estimation (i.e. symbol timing recovery) was performed by an interpolator that resampled the digitized signal dynamically. This interpolation filter was controlled by a feedback path consisting of a timing error detector and loop filter. In aggregate, these elements form a phase-locked loop (PLL) which keeps the decision timing synchronized with the captured data stream and corrects clock skew between the transmitter and receiver. This also was done in MATLAB, which implements interpolation with a piecewise parabolic interpolator [17], and implements timing error detection using the zero-crossing decision method [16]. In our experiment, the timing estimation PLL filter's bandwidth was one five hundredth of the symbol rate (owing to the near-zero frequency offset after carrier synchronization), the damping factor was 0.7, and the detector gain was unity.

Since our terminals were static, elevated, and the antennas were highly directive, our communication channel was very well behaved and can likewise be considered static. This is expected for future line-of-sight backhaul links which, like ours, will not suffer from blockage or dynamic multipath effects. Accordingly, channel estimation did not play a role in processing the received signal, and zero-forcing equalization was used to correct signal distortions. Though no data preamble was employed for this purpose, a small subset of the PRS sequence adequately served as a pilot for channel estimation and training. Future links will still need to account for outage probability due to heavy rainfall and will in some cases need to compensate for the variable atmospheric refractive index, but these effects take place on the timescale of minutes and likewise did not affect our data. Finally, the data was demodulated by

identifying the constellation points that produced the minimum error vector magnitudes to the received symbols.

B. AWG Source Results

Table I shows the approximate link budget for measurements when the AWG was used for signal generation.

TABLE I. LINK BUDGET OF DATA TRANSMISSION WITH AWG SOURCE

Transmit power	84 mW (19.24 dBm)
Antenna gain (Tx and Rx)	48 dBi
Atmospheric loss	8.2 dB
Free space path loss	144 dB
Intensity at Rx antenna	$7.56 \mu \text{W/m}^2 (-21.2 \text{dBm/m}^2)$
Antenna effective area (Rx)	0.0292 m ²
Captured power	221 nW (-36.6 dBm)
Conversion loss in Rx	11 dB
Total IF path gain	42 dB
Final digitized signal power	278 μW (-5.56 dBm)
Noise power spectral density	-148.5 dBm/Hz

Table II shows the experimental data transmission results for the same measurements. Bit error rates reported with a "less than (<)" symbol indicate no errors were detected in the demodulated data.

TABLE II. SUMMARY OF DATA TRANSMISSION WITH AWG SOURCE

Modul. Order M	Bandwidth (GHz)	Bit Rate (Gbps)	BER	SNR (dB) measured (predicted)	EVM (%) measured (predicted)
2	0.3913	0.301	< 3.59×10 ⁻⁶	27.5 (28.2)	4.2 (3.9)
2	0.7826	0.602	< 1.74×10 ⁻⁶	25.8 (25.2)	5.1 (5.5)
2	1.565	1.204	< 8.48×10 ⁻⁶	24.1 (22.2)	6.2 (7.8)
2	3.129	2.407	< 4.21×10 ⁻⁶	16.2 (19.1)	15.5 (11.1)
2	5.452	4.194	< 2.40×10 ⁻⁶	10.7 (16.7)	29.2 (14.6)
4	0.3193	0.602	< 1.80×10 ⁻⁶	28.0 (28.2)	4.0 (3.9)
4	0.7826	1.204	< 8.72×10 ⁻⁶	26.0 (25.2)	5.0 (5.5)
4	1.565	2.407	< 4.24×10 ⁻⁷	25.1 (22.2)	5.6 (7.8)
4	3.130	4.815	< 2.11×10 ⁻⁷	16.9 (19.1)	14.3 (11.1)
4	5.452	8.387	5.17×10 ⁻⁶	10.7 (16.7)	29.2 (14.6)

Four representative constellation diagrams are shown in Fig. 3. In all cases except the 8.387 Gbps-QPSK case the constellations reveal a comfortable error vector magnitude well within the bounds of the decision thresholds. The 8.387 Gbps-QPSK case is clearly at the boundary of low-error operation, even though it still exhibits a very acceptable BER of 5.17×10^{-6} , which could readily be improved with forward error correction. The 4.194 Gbps-BPSK constellation is also approaching the boundary of low-error operation. In these two cases, the signal-noise-ratio (SNR) is about 11 dB.

C. FPGA Source Results

Table II shows the data transmission results of two measurements where the FPGA was used for signal generation and Fig. 4 shows the constellation diagrams obtained.

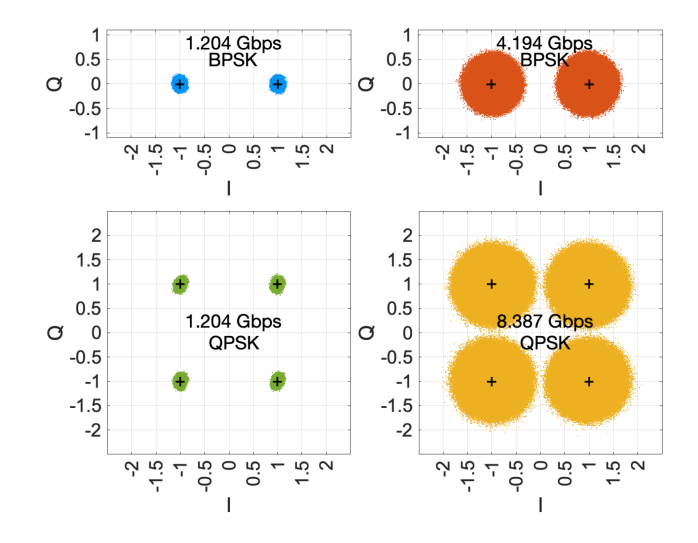


Fig. 3: Constellation diagrams for four different data rate and modulation cases, using the AWG as the signal source. BPSK = 2-PSK, QPSK = 4-PSK.

TABLE III. SUMMARY OF DATA TRANSMISSION WITH FPGA SOURCE

Modulation Order M	Bandwidth (GHz)	Bit Rate (Gbps)	BER	SNR (dB)
2	0.666	0.512	< 2.04×10 ⁻⁶	30.5
4	0.666	1.024	< 1.02×10 ⁻⁶	30.9

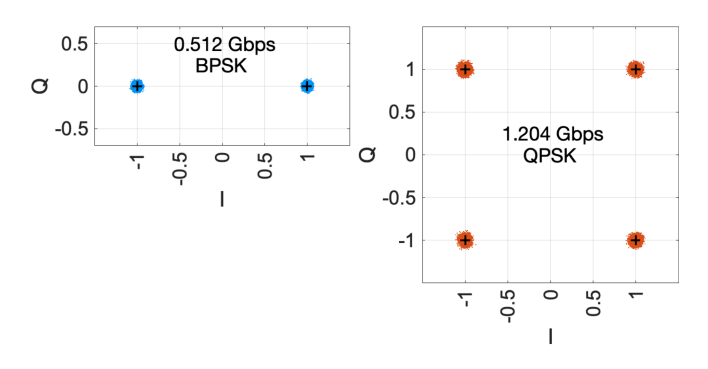


Fig. 4: Constellation diagrams for the BPSK and QPSK cases, using the FGPA as the signal source.

The plots reveal very favorable performance from the FPGA. However, we note that this is the result of some optimization efforts. Several previous configurations of the LO and IF frequencies did not result in clean (or even usable) data due to aliasing and spurious signals generated within the converters. Surprisingly, in this case the FPGA-sourced data exhibited SNRs up to almost 5 dB higher than data sourced from the

AWG. We hypothesize that this is a consequence of two major factors. First, cable losses are reduced for the lower IF frequency employed by the FPGA. Second, the upconverter, downconverter, and amplifier performance are also frequency dependent, and improve (i.e. exhibit lower loss or greater conversion efficiency) at lower IF frequencies.

IV. DISCUSSION

We can estimate the extent of channel effects including water vapor absorption and antenna vibrations on the link performance. These can be significant since operations occurred in far less than optimal conditions. Specifically, there was a strong south wind of about 7 m/s average speed (11 m/s peak gusts) that was particularly noticeable at Boomer Lake where the surrounding open expanse provided no shielding. A tall wall on the stadium roof provided some wind protection to the transmitter, though gusts of 8.5 m/s were still observed. Vibrations on both the transmitter and receiver modules could be visibly observed during measurements. However, both modules were aligned mostly parallel to the wind direction, which is a relatively stable configuration for the conditions. Though not measured in this campaign, we estimate from our observations and previous pointing jitter measurements that this accounted for no more than 1 dB of the effective loss. This quantifies a strong robustness to vibrations and minor antenna pointing errors for multi-kilometer terahertz links. On the other hand, the ambient temperature was 96 °F (36 °C), with 47-53% relative humidity, so that atmospheric water vapor was quite elevated (19.6-22.3 g/m³; higher at the lake). At 130 GHz, the calculated atmospheric absorption was 2.84-3.42 dB/km or 8.53-10.26 dB (total), which is very significant considering a 6 dB improvement in link budget enables a doubling of the communication range. This strongly suggests that our current system is already capable of 6 km or more of range in cooler seasons when the water vapor density is sharply decreased.

It is instructive to compare the performance of this system to similar demonstrations, such as that of Ref. [1]. Despite using less transmitted power and propagating over a 50% greater range, we obtained a bit rate improvement of >100%. While several factors certainly account for this, we suggest a few of possibly greater importance. First the relative simplicity of our system is suspected to result in fewer nonlinear mixing spurs in the transmitted and downconverted signals, resulting in a lower effective noise. In our experience, these are encountered often due to the non-idealities of the nonlinear components. To optimize system performance, such spurs need to be minimized by careful selection of LO and sampling frequencies, utilization of filters, and adjustment of component gains where possible. The greater number of mixers and/or multipliers in more complex systems compounds such problems. Second, the performance of our custom Cassegrain antennas appears to be closer to the design specification than those utilized in Ref. [1]. This may account for 6 dB or more improvement in the overall link budget. Third, our carrier frequency of 130 GHz is much less susceptible to atmospheric absorption. While the weather conditions in Ref. [1] were not reported, if the water vapor density was similar, their total absorption loss would have been significantly greater (~10 dB).

We also mention a significant challenge we observed in utilizing FPGAs, which are a current approach to transition our system to real-time operation. The relatively low sampling rates of FPGAs (specifically, the RF System-On-Chip sample rate of 6 Gsps) compared to the AWG or DSO (64+ Gsps) introduce numerous, closely spaced signal images in the transmitted frequency spectra. Spurious mixing products within the upconverter and downconverter increase the number of such images, often at unpredictable and inconvenient frequencies. This leads to signal aliasing that can be difficult to prevent with simple, low-loss filters. Again, we found that judicious choice of LO frequencies is a partial solution. However, this represents a growing challenge for the future when numerous RF channels of the FPGA must be multiplexed to achieve signal bandwidths exceeding 3 GHz.

Our results reveal that COTS equipment is already adequate to achieve > 3 km ranges for backhaul links approaching 10 Gbps, even in difficult weather conditions. While these experiments are promising, we estimate that the same equipment is capable of significantly higher performance. One improvement is to address the LNA between the downconverter and DSO. While this amplifier's noise figure was specified at 2 dB, in practice it performed much worse (14 dB). It is not the first element in the receiver chain, however, so replacing it would only represent a small SNR improvement of about 0.3 dB overall. Second, an off-axis parabolic reflector antenna design could add 4-6 dB overall by preventing signal blocking in the Cassegrain subreflectors, a particular problem at the transmitter. We are currently in the process of testing such antennas. Third, downconverter conversion loss represents an unavoidable penalty of 11 dB. While the downconverter's internal amplifier reverses this (12 dB gain), it also has a noise figure of 13 dB. An upstream broadband LNA operating at the carrier frequency could improve the overall system noise figure by 6 dB and is already commercially available. However, more generally, improvements in the design of low-noise waveguide amplifiers would significantly increase the capabilities of current systems. Combining these improvements, the system link budget could be improved by 10-12 dB, which would enable communication performance similar to what we have currently observed, but over distances exceeding 10 km. Forward error correction would provide even more margin for success.

V. CONCLUSION

The results presented here demonstrate the immediate potential for high bit-rate wireless backhaul over long distance (>3 km) using commercially available RF components operating at terahertz frequencies. Our system was able to achieve 8.387 Gbps with a very acceptable BER of 5.17×10⁻⁶ over a range of 2.92 km in challenging weather conditions (high atmospheric water vapor density and strong wind). Future improvements in the system architecture and antennas should enable similar communications over distances exceeding 10 km, all while mostly utilizing COTS equipment. This translates into significant real-world utility for prospective wireless backhaul applications. We have also qualified the usage of an FPGA in place of the AWG instrument, revealing that spectrum aliasing is a significant challenge compounded by spurious mixing products and low sampling rates inherent in COTS equipment. The next major hurdle in the deployment of such systems is to address these difficulties and also achieve real-time operations with FPGAs or application-specific integrated circuits. Work toward overcoming the challenges of COTS FPGAs is currently underway.

ACKNOWLEDGMENT

The authors thank Azmeen Rahman for his assistance in designing the Cassegrain antennas used in this work.

REFERENCES

- P. Sen, J. V. Siles, N. Thawdar, and J. M. Jornet, "Multi-kilometre and multi-gigabit-per-second sub-terahertz communications for wireless backhaul applications," Nature Electronics, vol. 6, pp. 164-175, 2023, DOI: 10.1038/s41928-022-00897-6.
- [2] P. K. Singya, B. Makki, A. D'Errico, and M.-S. Alouini, "Hybrid FSO/THz-based backhaul network for mmWave terrestrial communication," IEEE Transactions on Wireless Communications, vol. 22, pp. 4342-4359, 2023, DOI: 10.1109/TWC.2022.3224331.
- [3] V. U. Pai, P. Bhardwaj, and S. M. Zafaruddin, "Performance analysis of dual-hop THz wireless transmission for backhaul applications," 2021 IEEE Intl. Conference on Advanced Networks and Telecomm. Systems (ANTS), 13-16 Dec. 2021, DOI: 10.1109/ANTS52808.2021.9937036.
- [4] T. Kürner, D. M. Mittleman, and T. Nagatsuma, eds., THz Communications, Springer Series in Optical Sciences, no. 234, Springer 2022.
- [5] E. Yaacoub and M.-S. Alouini, "Efficient fronthaul and backhaul connectivity for IOT traffic in rural areas," IEEE Internet of Things Mag., vol. 4, pp. 60-66, 2021, DOI: 10.1109/iotm.0001.1900061.
- [6] I. F. Akyildiz, J. Jornet, and C. Han, "Terahertz band: next frontier for wireless communications," Phys. Comm., vol. 12, pp. 16-32, 2014, DOI: 10.1016/j.phycom.2014.01.006
- [7] A.-A. A. Boulogerogos, et al.,, "Terahertz technologies to deliver optical network quality of experience in wireless systems beyond 5G,"

- IEEE Comm. Mag., vol. 56, pp. 144-151, 2018, DOI: 10.1109/mcom.2018.1700890.
- [8] W. Jiang, B. Han, M. A. Habibi, and H. D. Schotten, "The road toward 6G: a comprehensive survey," IEEE Open J. Comun. Soc., vol. 2, pp. 334-336, 2021, DOI: 10.1109/mc.2016.245.
- [9] J. Ma, et al., "Security and eavesdropping in terahertz wireless links," Nature, vol. 563, pp. 89-93, 2018, DOI: 10.1038/s41586-018-0609-x.
- [10] D. Heligman, Z. R. Spencer, and R. Mendis, "Terahertz imaging through fog," Conference on Lasers and Electro-Optics (CLEO) 2023, pp. 1-2, California, USA.
- [11] Z. R. Spencer, D. Heligman, and R. Mendis, "Terahertz imaging through dust," IEEE Research and Applications in Defense (RAPID) Conference 2024, Florida, USA.
- [12] K. Su, L. Moeller, R. B. Barat, and J. F. Federici, "Experimental comparison of performance degradation from terahertz and infrared wireless links in fog," J. Opt. Soc. Am. A, vol. 29, p. 172, 2012, DOI: 10.1364/josaa.29.000179.
- [13] J. F. Federici, K. Su, L. Moeller, and R. B. Barat, "Experimental comparison of terahertz and infrared data signal attenuation in dust clouds," J. Opt. Soc. Am. A, vol. 29, pp. 2360-2366, 2012, DOI: 10.1364/josaa.29.002360.
- [14] J. Ma, F. Vorrius, L. Lamb, L. Moeller, and J. F. Federici, "Experimental comparison of terahertz and infrared signaling in laboratory-controlled rain," J. Infrared Millim Terahertz Waves, vol. 36, pp. 856-865, 2015, DOI: 10.1007/s10762-015-0183-3.
- [15] K. Strecker, W. Choi, and J. O'Hara, "A wideband millimeter-wave communication and sensing testbed for 75-500 GHz," in 2023 IEEE Texas Symposium on Wireless and Microwave Circuits and Systems (WMCS), 2023, pp. 1-5, DOI: 10.1109/WMCS58822.2023.10194272.
- [16] U. Mengali and A. N. D'Andrea, "Synchronization Techniques for Digital Receivers," New York: Plenum Press, 1997.
- [17] M. Rice, "Digital Communications: A Discrete-Time Approach," Upper Saddle River, NJ: Prentice Hall, 2008.